Journal of Materials Chemistry C

PAPER

View Article Online
View Journal | View Issue

Cite this: J. Mater. Chem. C, 2017, 5, 1685

Europium-decorated ZnO quantum dots as a fluorescent sensor for the detection of an *anthrax* biomarker

Rui Zhou,[a] Qi Zhao,*[a] Kai-Kai Liu,[bc] Ying-Jie Lu,[a] Lin Dong[a] and Chong-Xin Shan*[ab]

Received 24th November 2016,
Accepted 20th January 2017

DOI: 10.1039/c6tc05108a

rsc.li/materials-c

A hybrid nanostructure based on ZnO quantum dots (QDs) has been fabricated for ratiometric detection of *Bacillus anthracis* spores, where yellow-emitting ZnO QDs are employed as the internal reference and europium ions (Eu^{3+}) are chelated on the surface of the ZnO QDs as the signal report unit. The Eu^{3+} exhibits enhanced red luminescence upon bonding with calcium dipicolinate (CaDPA), an important biomarker of *Bacillus anthracis* spores, while the fluorescence of the ZnO QDs will not be altered. Accordingly, increased CaDPA levels can lead to variation of the two fluorescence intensity ratios of the ZnO/Eu hybrid nanostructure. The time-dependent fluorescence response reveals that the reaction can be completed within 8 s, thus enabling the rapid detection of *Bacillus anthracis* spores. The detection limit for CaDPA is 3 nM, which is six orders of magnitude lower than an infectious dosage of *Bacillus anthracis* spores for human beings (60 μM). In addition, the sensor shows a remarkable selectivity for CaDPA over other aromatic ligands, amino acids and common cellular ions. The fast response speed as well as good sensitivity and selectivity means the ZnO/Eu nanostructure has great potential applications in clinical analysis.

1 Introduction

In 2001, the United States suffered a biological attack with *Bacillus anthracis* (*B. anthracis*) spores, and this potential biological warfare agent has received particular attention all over the world since then.[1,2] Recently, *anthrax* has remained one of the most dangerous and terrible chemical and biological weapons. Upon inhalation of more than 10^4 *B. anthracis* spores, even with drug treatment the mortality rate is still up to 75% within 24–48 hours.[3,4] Because of its high lethality, rapid and sensitive detection of *B. anthracis* spores is of great significance and importance for controlling *anthrax* disease and preventing biological attacks.

During the past decades, many detection methods have been developed by using various analytical techniques such as the polymerase chain reaction (PCR),[5,6] immunoassays,[7] surface enhanced Raman spectroscopy (SERS),[8] and lanthanide-based luminescence techniques.[9] PCR and immunoassays as traditional biological methods usually require lengthy cycles, complicated operation, expensive reagents and professional analysis. Recently, optical methods including SERS and luminescence techniques have attracted a great deal of interest because of their low cost, rapid response and easy operation. Generally, optical sensing of bacterial spores is based on the detection of calcium dipicolinate (CaDPA), a unique biomarker and major component of *Bacillus* spores.[10] It is noteworthy that lanthanide ions (Ln^{3+}) exhibit highly enhanced luminescence upon bonding with CaDPA due to the antenna effect.[11,12] Moreover, the luminescence of Ln^{3+} has unique features including large Stokes shift, narrow emission bands, and long fluorescence lifetime.[13,14] Therefore, lanthanide ion-functionalized fluorescent sensors have been considered a promising method for the rapid, sensitive and selective detection of CaDPA. To date, some lanthanide ion-based sensing platforms have been prepared such as nanoparticles,[14] carbon nanotubes,[15] solid films,[9,16] and metal organic frameworks.[17] However, the concentration of CaDPA is usually measured by luminescence variation alone in most of the lanthanide-based sensors. In such a case, it is difficult to judge whether signal enhancement is due to a target-induced increase or operation errors, or instrumental or environmental factors, especially at very low CaDPA concentrations. Alternatively, dual-emission ratiometric fluorescent sensors are supposed to be more appealing,[10,18–20] where the analyte CaDPA can be determined by the luminescence ratio between the analyte signal and the reference signal. The built-in correction of the ratiometric design effectively eliminates the potential operation and environmental effects, thus significantly improving the sensitivity and accuracy of the sensors.

[a] School of Physical Engineering, Zhengzhou University, Zhengzhou 450052, China. E-mail: zhaoqiv@126.com, cxshan@zzu.edu.cn
[b] State Key Laboratory of Luminescence and Applications, Changchun Institute of Optics, Fine Mechanics and Physics, Chinese Academy of Sciences, Changchun, 130033, China
[c] University of Chinese Academy of Sciences, Beijing, 10049, China

Zinc oxide (ZnO) quantum dots (QDs) have been exhaustively investigated in many fields, such as light-emitting devices,[21] lasers,[22] photodetectors,[23] gas sensors,[24] solar cells,[25] *etc.*,[26,27] due to their unique optical and electrical properties.[28,29] Compared with traditional semiconductor QDs (CdSe, CdS, *etc.*), ZnO QDs are less expensive, eco-friendly, favorably biocompatible and low cytotoxicity.[30,31] Recently, their excellent fluorescence properties including high quantum yield, strong photoluminescence emission and resistance to photobleaching have inspired researchers to use ZnO QDs in drug delivery,[32] biological labeling[33] and biosensing.[34,35] However, no reports on a fluorescent sensor for *B. anthracis* using ZnO QDs as an internal reference can be found.

In this paper, ZnO QDs functionalized with (3-aminopropyl) triethoxysilane (APTES) have been prepared. These APTES-capped ZnO QDs are endowed with functional groups, strong luminescence, large surface areas and enhanced dispersibility in aqueous solution, which facilitates the development of strategies using ZnO QDs as the reference signal in dual-emission fluorescent sensors. Subsequently, europium ions (Eu^{3+}) were selected and chelated onto the surface of the ZnO QDs as the sensing moiety, considering that the strongest emission of Eu^{3+} at around 616 nm will not be interfered with by the ZnO QD emission. The fluorescence of Eu^{3+} will be sensitively responsive to CaDPA while the inner ZnO QDs are inert, which enables ratiometric and visual detection of bacterial spores without expensive equipment. Because of the CaDPA-inert fluorescence of the ZnO QDs, the efficient sensitization of CaDPA to lanthanide, and the narrow-band emissions of Eu^{3+}, these europium-decorated ZnO QD sensors exhibit a remarkable limit of detection (3 nM) towards CaDPA and outstanding selectivity over aromatic ligands in aqueous solution.

2 Experimental section

2.1 Materials

All the chemicals used in this paper were analytical grade without further purification: zinc acetate dihydrate ($Zn(OAc)_2{\cdot}2H_2O$), (3-aminopropyl) triethoxysilane (APTES), ethylenediamine tetraacetic acid dianhydride (EDTAD), 2,6-pyridinedicarboxylic acid (DPA), europium oxide and potassium hydroxide (KOH) were purchased from Aladdin Chemistry Co. Ltd (Shanghai, China). Dimethylacetamide (DMAC), disodium hydrogen phosphate dodecahydrate and trisodium citrate dihydrate were purchased from Sinopharm Chemical Reagent Co. Ltd (Shanghai, China). L-Glutamic acid and calcium hydroxide were purchased from Tianjin Damao Chemical Reagent Factory (Tianjin, China). Phthalic acid and benzoic acid were purchased from Tianjin Sheng Ao Chemical Reagent Co. Ltd (Tianjin, China). Absolute ethanol was purchased from Tianjin Yongda Chemical Reagent Co. Ltd (Tianjin, China). Concentrated nitric acid was purchased from Luoyang Chemical Reagent (Luoyang, China). Calcium dipicolinate (CaDPA) was synthesized with DPA and calcium hydroxide according to the method demonstrated in the literature.[10]

2.2 Preparation

2.2.1 Synthesis and functionalization of ZnO QDs. 25 mM $Zn(OAc)_2{\cdot}2H_2O$ was dissolved in 150 mL ethanol and refluxed under continued stirring for 2 h at 80 °C. A 35 mM KOH solution was dissolved in 20 mL ethanol by sonication for 30 min. The KOH solution was added dropwise into the $Zn(OAc)_2{\cdot}2H_2O$ solution for 30 min at 0 °C. To obtain amino-functionalized ZnO QDs, a mixture of 1.5 mL deionized water and 500 μL APTES was added into the above solution under continuous stirring for 5 h at room temperature. Afterwards, the precipitate was collected by centrifugation at 6000 rpm for 10 min and washed with absolute ethanol three times. Finally, the precipitate (ZnO QDs) was dried in a blast oven at 60 °C for 2 h.

2.2.2 Europium modification of ZnO QDs. The ZnO QDs (0.5 g) were put into a 100 mL round-bottomed flask. EDTAD (0.25 g) was dissolved in dimethylacetamide (30 mL). Next, the prepared EDTAD solution was added dropwise into the flask containing the ZnO QDs followed by continuous stirring for 12 h at 60 °C under a nitrogen atmosphere. The precipitate was collected by centrifugation and washed with DMAC three times to remove unreacted materials, and finally absolute ethanol once to dry the sample. Subsequently, the complex was dispersed in pH = 9.6 sodium/bicarbonate buffer (30 mL) and stirred for 2 h. The reaction product was centrifuged and washed with deionized water until the supernatant showed neutral pH. Then the product was dispersed in a 0.01 M $Eu(NO_3)_3$ aqueous solution (30 mL) and stirred for 2 h. The produced [ZnO(EDTA)Eu] nanostructures (labelled as ZnO/Eu) were centrifuged and washed with deionized water, until Eu^{3+} could not be detected in the supernatant. Finally, the ZnO/Eu nanostructures were dried in a blast oven at 60 °C for 2 h.

2.2.3 Preparation of CaDPA. 3.3 mM DPA and an equal molar amount of $Ca(OH)_2$ were dissolved in 50 mL of deionized water separately. Then the $Ca(OH)_2$ aqueous solution was added dropwise into the DPA solution. The mixed solution was stored at 5 °C for 48 h. Afterwards, the precipitates were obtained by filtering and drying at 60 °C for 6 h.

2.2.4 CaDPA detection using the ZnO/Eu nanostructures. In a typical run, ZnO/Eu nanostructures were dispersed with a final concentration of 0.5 mg mL^{-1} in aqueous solution, and then reacted with standard CaDPA solutions. The fluorescence intensity of the mixture was monitored at 530 nm and 616 nm under a 280 nm excitation wavelength in order to investigate the relationship between the intensity ratio I_{616}/I_{530} and the concentration of CaDPA ranging from 0 to 4 μM.

2.3 Characterization

The X-ray diffraction (XRD) pattern of the ZnO QDs was recorded using an X′Pert Pro diffractometer, in which X-rays were generated by a Cu Kα source. A JEM-2010 transmission electron microscope (TEM) was employed to characterize the size and crystallinity of the QDs. The fluorescence spectra of the ZnO QDs and ZnO/Eu nanostructures were obtained with an F-7000 fluorescence spectrophotometer. The UV-Vis absorption of the ZnO QDs and CaDPA was obtained using a UH4150

spectrophotometer. Fourier transform infrared (FTIR) spectra of the samples were recorded on a Thermo Scientific Nicolet iS10 FTIR spectrometer from dry KBr discs, over the range 4000–400 cm^{-1}. The X-ray photoelectron spectroscopy (XPS) spectra of the samples were collected by using a Thermo Fisher Scientific ESCALAB 250Xi spectrometer equipped with an Al Kα X-ray radiation source, and the XPS binding energy was internally referenced to the C 1s peak (BE = 284.8 eV). Absolute photoluminescence quantum yields (QY) were measured by an absolute PL quantum yield measurement system (C9920-02, Hamamatsu Photonics K. K., Japan).

3 Results and discussion

3.1 Preparation of ZnO QDs

Scheme 1 illustrates the preparation process of the ZnO/Eu nanostructures and the mechanism for CaDPA detection. Firstly, ZnO QDs were prepared, from which yellowish emission could be detected under UV illumination. Subsequently, EDTAD was covalently bonded to the ZnO QDs *via* a dehydration condensation reaction between the amino and the carboxylic anhydride groups. Finally, Eu^{3+} was anchored on the surface to obtain the ZnO/Eu nanostructures, in which the Eu^{3+} could be sensitized by CaDPA.

As shown in Fig. 1a, all the XRD peaks of the as-prepared ZnO QDs can be readily indexed to wurtzite ZnO (JCPDS 89-1397).[36] A panoramic TEM image (Fig. 1b) shows that the ZnO QDs consisted of nanospheres with an average diameter of 5 nm. The HRTEM image of an individual QD shows clear lattice fringes with a distance of around 0.281 nm, which corresponds to the inter-planar distances of the (100) planes of wurtzite ZnO (inset in Fig. 1b).[35] The obvious lattice fringes confirm the high crystallinity of the ZnO QDs. The inset in Fig. 1c is a photograph of the ZnO QDs in daylight (left) and under a UV lamp at 365 nm (right). The aqueous dispersion of the ZnO QDs is clear and transparent in daylight, indicating that the as-prepared QDs are well water-soluble. And under UV-light irradiation, the ZnO QDs exhibit strong yellow luminescence. The corresponding emission spectrum is composed of a strong band peaking at 530 nm, and

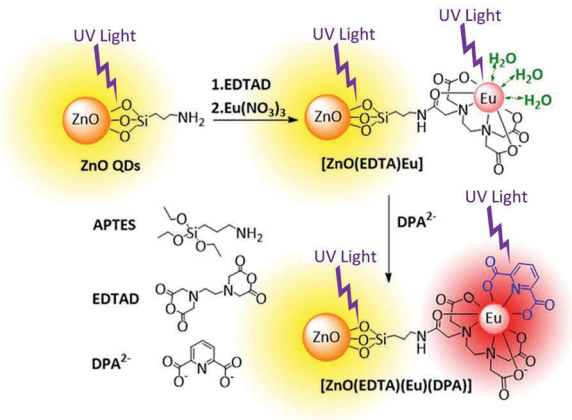

Scheme 1 Schematic illustration of the preparation of the ZnO/Eu nanostructure and the sensing mechanism for CaDPA.

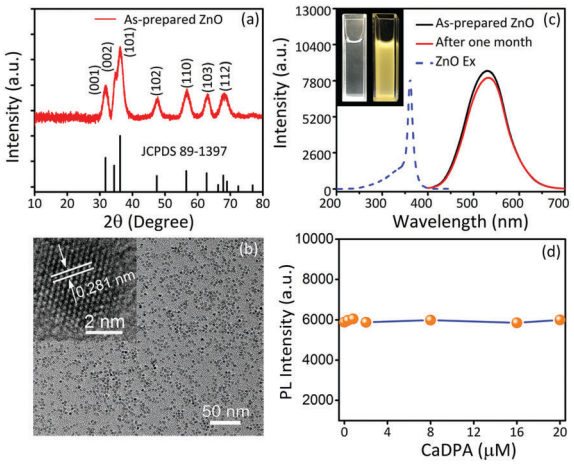

Fig. 1 (a) XRD pattern of the as-prepared ZnO QDs. (b) TEM and HRTEM (the inset) image of ZnO QDs. (c) The excitation spectrum (dot line) of the ZnO QDs and emission spectrum of the freshly prepared QD aqueous dispersion (black solid line) and sample after being stored for 1 month (red solid line). Inset: Photograph of the ZnO QDs in daylight (left) and under a UV lamp at 365 nm (right). (d) The fluorescence intensity response curve of the ZnO QDs at 530 nm *versus* concentration of CaDPA.

the ZnO sample exhibits an excitation band ranging from 250 to 380 nm (the dot line in Fig. 1c). In addition, the sample shows slight changes in luminescence intensity after being stored under chamber conditions for one month (Fig. 1c). These results indicate that the ZnO QDs have good colloidal and optical stabilities. Importantly, the fluorescence intensity of the ZnO QDs is invariable after introducing various amounts of CaDPA, indicating that their fluorescence intensity is independent of the CaDPA concentration (Fig. 1d). On the basis of the above experimental results, it is deemed that the ZnO QDs can be used as the fluorescence reference in a ratiometric sensor for the detection of CaDPA.

3.2 Europium modification of ZnO QDs

As the signal report unit, Eu^{3+} is grafted onto the surface of the ZnO QDs through the chelating agent EDTA. The FTIR spectrum of the ZnO QDs illustrated in Fig. 2a shows a broad absorption band at 3425 cm^{-1}, which belongs to the stretching vibration of N–H. The peak at 2936 cm^{-1} can be attributed to the characteristic stretching vibration of C–H. The N–H and the C–H bending peaks appear at 1574 cm^{-1} and 1405 cm^{-1}, respectively. The band at 1018 cm^{-1} is due to the stretching vibration of Si–O. In addition, the peak at 525 cm^{-1} belongs to the stretching vibration of Zn–O. These results indicate that ZnO QDs are well modified by APTES.[31] Compared to the ZnO QDs, additional peaks are observed at 1637 cm^{-1} and 1506 cm^{-1} for the ZnO/Eu nanostructures, and the former can be attributed to the stretching vibration of the amide bond formed between the amino and carboxylic groups, while the latter to the symmetric stretching of COO^{-} in EDTA.[37] These results demonstrate that the ZnO/Eu hybrid nanostructures have been fabricated.

Furthermore, XPS spectra are collected to determine the chemical compositions of the ZnO QDs and ZnO/Eu nanostructures, as shown in Fig. 2b. Both the ZnO QDs and ZnO/Eu

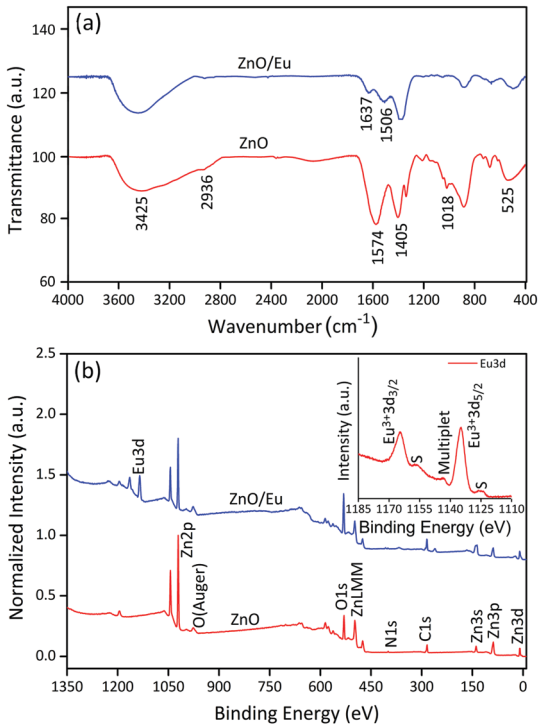

Fig. 2 (a) FTIR spectra of the ZnO QDs (red) and ZnO/Eu nanostructures (blue). (b) XPS spectra of the ZnO QDs and ZnO/Eu nanostructures. Inset: XPS Eu 3d core level spectrum of the ZnO/Eu sample.

Table 1 Elemental analysis results of the ZnO QDs and ZnO/Eu nanostructure observed by X-ray photoelectron spectroscopy

	Elemental atomic percentage (wt%)					
Sample	C	O	N	Si	Zn	Eu
ZnO QDs	8.19	12.05	1.66	3.75	74.35	—
ZnO/Eu	6.38	21.93	2.35	2.24	44.55	22.55

nanostructures contain the elements Zn, C, N and O.[38] It is noteworthy that the Eu element arises in the ZnO/Eu nanostructures. The high-resolution spectrum of Eu 3d (inset in Fig. 2b) exhibits two contributions, $3d_{3/2}$ and $3d_{5/2}$ (resulting from the spin–orbit splitting), located at 1165 eV and 1134 eV, respectively. Additional peaks at 1156 eV and 1124 eV are due to the shake-down satellites of Eu^{3+} $3d_{3/2}$ and Eu^{3+} $3d_{5/2}$, respectively.[39,40] A satellite peak arises at 8.5 eV higher binding energy relative to the Eu $3d_{5/2}$ main structure, as is reported in the literature.[39] The atomic concentrations of the ZnO QDs and ZnO/Eu nanostructures are shown in Table 1. The XPS results further confirm the composition of the ZnO QDs and ZnO/Eu nanostructures, which is in good agreement with FTIR results.

3.3 Feasibility of the ZnO/Eu for CaDPA sensing

To evaluate the dual-emission performance of the ZnO/Eu hybrid nanostructures, the luminescence spectra of the [Eu(DPA)] complexes have been recorded, as shown in Fig. 3a. The excitation spectrum of [Eu(DPA)] is dominated by a sharp line at around 280 nm. Under the excitation of 280 nm light, intense and characteristic emission patterns of the Eu^{3+} can be yielded, as evidenced in Fig. 3a. These emission lines can be explicitly assigned to the transition of $^5D_1$–^7F_J (J = 0, 1) and $^5D_0$–^7F_J (J = 0, 1, 2, 3 and 4), respectively.[41,42] The strongest red emission locates at around 616 nm, which will not be interfered with by the ZnO QD emission at 530 nm. In addition, the aqueous solution of ZnO QDs shows a broad absorption band in the deep UV region (Fig. 3b), which matches well with the absorption peak of CaDPA at 280 nm (Fig. 3b), suggesting that the ZnO QDs and [Eu(DPA)] complexes can be simultaneously excited at a wavelength of 280 nm. According to the above results, the ZnO/Eu nanostructures are expected to achieve dual-emission detection of CaDPA. To verify this speculation, the response of the ZnO/Eu nanostructures towards CaDPA has been observed in the presence of a 16 μM solution of CaDPA. The emission and excitation spectra of the mixed solution are displayed in Fig. 3c. By monitoring the characteristic emissions of the Eu^{3+} and ZnO QDs at 616 nm and 530 nm, two excitation bands are obtained which overlap with several sharp lines (616 nm and 593 nm) coming from Eu^{3+} and a broad band (530 nm) from ZnO QDs. In addition, the quantum yields for the ZnO/Eu hybrid nanostructures in the absence and presence of DPA were measured to be 1.89% and 10.69%, respectively. Accordingly, the ZnO/Eu nanostructures can work effectively as a dual-emission sensor for CaDPA.

3.4 Sensing properties of the ZnO/Eu toward CaDPA

Considering that inhaled anthrax disease causes harm to human health in a very short time, the response time is critical for an anthrax sensor. The time-dependent fluorescence response of the ZnO/Eu nanostructures to CaDPA solution is monitored at 616 nm with excitation at 280 nm (Fig. 4). The curve shows that the fluorescence intensity increases to the maximum value in 8 s and stays at the maximum value after 8 s, enabling rapid detection of anthrax spores. The fast response time is partially attributed to the high affinity between DPA^{2-} and Eu^{3+}. Another important reason is the larger surface-to-volume ratio of the 5 nm-diameter ZnO QDs, enhancing contact between CaDPA and the nanostructures.

To evaluate the sensitivity of the ZnO/Eu nanostructure sensor, CaDPA solutions with different concentrations were employed as the sensing specimen as indicated in Fig. 5. The fluorescence intensity of the ZnO/Eu nanostructures increases linearly with the concentration of CaDPA in the investigated range from 0 to 4 μM (R^2 = 0.99585, Fig. 5b). The limit of detection (LOD) for CaDPA is calculated to be 3 nM according to the method suggested by IUPAC.[48,49] This value is over six orders of magnitude lower than an infectious dosage of *B. anthracis* spores (60 μM) for human beings. Interestingly, the color change can be identified unaided by eye under UV illumination, even at a CaDPA concentration as low as 0.5 μM. As is shown in Table 2, the limit of detection and response time of the ZnO/Eu-based method are quite competitive compared to the developed optical detection method for *Bacillus anthracis*.

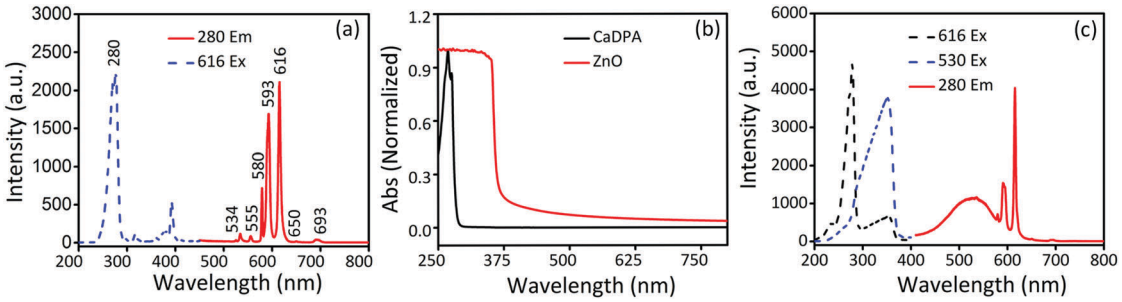

Fig. 3 (a) The excitation (blue) and emission (red) spectra of [Eu(DPA)] complexes. (b) UV-Vis absorption spectra of ZnO QDs (red) and 1 mM CaDPA aqueous solution (black). (c) The excitation and emission spectra of the ZnO/Eu nanostructures in the presence of a 16 μM solution of CaDPA.

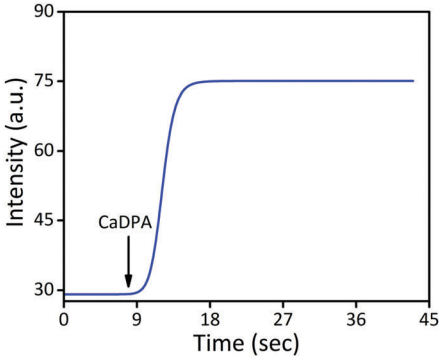

Fig. 4 Time-dependent fluorescence intensity curve of the sensor following exposure to CaDPA (fluorescence detected at 616 nm).

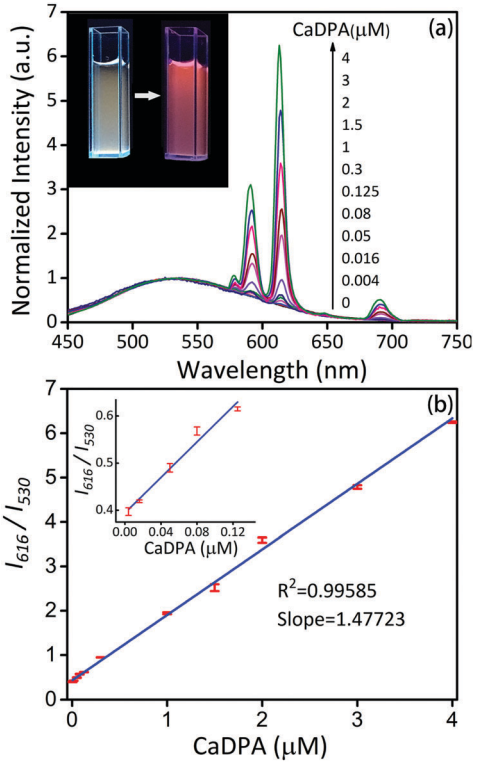

Fig. 5 (a) Fluorescence emission spectra of the ZnO/Eu nanostructures in the presence of CaDPA with different concentrations (0, 0.004, 0.016, 0.05, 0.125, 0.3, 1, 1.5, 2, 3, 4 μM). Inset: Photograph of the ZnO/Eu nanostructures dispersed in aqueous solution (left) and 0.5 μM CaDPA solution (right) under a UV lamp at 254 nm. (b) Ratiometric calibration curve of the sensor as a function of CaDPA concentration. The inset is an amplified spectrum of the ratiometric calibration curve of the sensor at low CaDPA concentrations. Error bars represent ±1 standard deviation from the mean, n = 5.

The highly sensitive detection of CaDPA can be attributed to three factors. Firstly, the luminescence of Eu^{3+} can be effectively sensitized by DPA through the antenna effect. Normally, the RE ions have low absorption cross section due to the forbidden 4f–4f transitions. Upon coordination with DPA ligands, the luminescence of the RE ions can be greatly enhanced. The DPA molecules will absorb the excitation energy efficiently and transfer it to the RE ions subsequently due to the good energy level matching between the triplet state (T1) of the ligand and the lowest excitation state of the RE ion, which is the so-called antenna effect.[11,12] Moreover, the 616 nm emission line is produced by the hypersensitive transition of Eu^{3+}, $^5D_0$–$^7F_2$, which is strongly dependent on the coordination environment of Eu^{3+}.[50] Secondly, the [ZnO(EDTA)] can exclude water molecules coordinated with Eu^{3+}, thus decreasing the non-radiative quenching. In the case of free Eu^{3+} as a sensor, water molecules will coordinate with Eu^{3+} forming [(H_2O)(Eu)(DPA)] complexes at low CaDPA concentrations, which can quench the Eu^{3+} luminescence.[51] By contrast, [ZnO(EDTA)] can replace part of the H_2O molecules to form [ZnO(EDTA)(Eu)(DPA)] complexes because of its prior affinity for rare earth ions, which can minimize the nonradiative quenching and eventually enhance the emission luminescence of Eu^{3+}.[19] Therefore, the chelation of Eu^{3+} on the ZnO QD surface can significantly improve the sensitivity of the nanoprobe, especially at low concentrations of DPA, compared to free europium ions. Thirdly, the large surface area and good dispersibility of the ZnO QDs provide abundant active sites for the DPA, leading to an increased frequency of contact with the DPA. Thus, the ZnO/Eu nanostructure sensor has high sensitivity to CaDPA.

Selectivity is another critical parameter for chemical sensors. Hence, the fluorescence response of the sensor towards several interfering substances has been investigated, including aromatic ligands, representative amino acids and common cellular ions such as benzoic acid, phthalic acid, citric acid, glutamic acid, L-phenylalanine, and aspartic acid, as well as Na^+, K^+, Ca^{2+}, Fe^{3+}, Cl^- and CO_3^{2-}, each at 20 μM concentration. These compounds

Table 2 Comparative study of the lanthanide ion-functionalized fluorescent sensors with different materials

Material	LOD[a]	Time[b]	Ref.[c]
A supramolecular monolayer	25 nM	10 min	M. D. Yilmaz *et al.*[43]
Bio-metal–organic frameworks	34 nM	20 s	Y. Zhang *et al.*[44]
Silver nanoparticles	10 nM	10 min	H. Tan *et al.*[45]
A PVA film	100 nM	—	B. Ma *et al.*[16]
Pentylamide-APS-EDTA-Tb coated silica nanoparticles	25 nM	—	K. M. L. Taylor *et al.*[46]
Carbon nanotubes	1 μM	3 s	C. Tan *et al.*[15]
Nanoscale metal–organic frameworks	48 nM	—	W. J. Rieter *et al.*[47]
Fluorescein isothiocyanate dye-doped silica nanoparticles	0.2 nM 10 pM	30 s 5.2 s	K. Ai *et al.*[14]
Graphene quantum dots	50 pM 10 pM	7.7 s	J. Ryu *et al.*[19]
PAN nanoparticles	50 pM 0.1 nM	20 s	W. K. Oh *et al.*[18]
A PES film	0.5 nM	50 s	I. Lee *et al.*[9]
ZnO QDs	3 nM	8 s	This work

[a] LOD means limit of detection. [b] Time means response time. [c] Ref. means reference number cited in the main text.

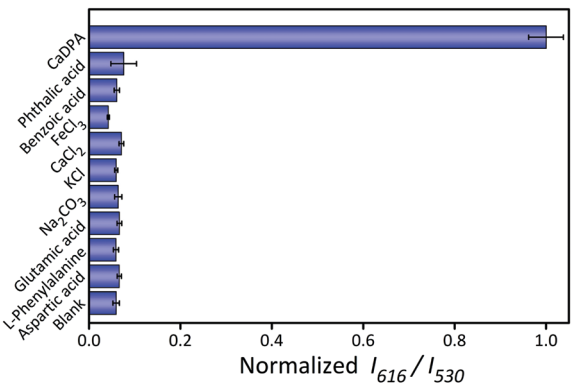

Fig. 6 The relative signal response (variation of I_{616}/I_{530} value) of the sensor toward CaDPA and various potential interfering substances. Error bars represent ±1 standard deviation from the mean, n = 5.

are selected because of their structural similarity with DPA^{2-} or potential presence in biological environments. All the samples are tested under identical conditions with the fluorescence response demonstrated in Fig. 6. Slight or negligible fluorescence changes are observed for the interfering groups. Only CaDPA exhibits a noteworthy fluorescence enhancement, indicating that the ZnO/Eu hybrid nanostructure sensor has good selectivity towards *B. anthracis* spores.

4 Conclusions

In summary, a ZnO/Eu nanostructure sensor for bacterial spores has been obtained by employing yellow-emitting ZnO QDs as the internal reference and red-emitting Eu^{3+} coordinated on the surface of the ZnO QDs as the sensing unit. The sensor shows dual emissions under the excitation of 280 nm light. Here, the increased CaDPA concentration can lead to red fluorescence enhancement of Eu^{3+} but the emission from the ZnO QDs is unchanged. The time-dependent fluorescence response of the dual-emitting sensor reveals that the reaction can be completed within 8 s, thus enabling rapid detection of *B. anthracis* spores. The detection limit for CaDPA is 3 nM, which is over six orders of magnitude lower than an infectious dosage of *B. anthracis* spores (60 μM) for human beings. In addition, the sensor shows remarkable selectivity for CaDPA over other aromatic ligands, amino acids and common cellular ions. More attractively, the target responsive fluorescence color change can be used for visual detection of CaDPA by unaided eyes. Therefore, the results reported in this paper may provide a route to a rapid and sensitive sensor of *B. anthracis* spores, which is of great significance in clinical analysis.

Acknowledgements

This work was financially supported by the Natural Science Foundation of China (21601159 and 11374296), the China Postdoctoral Science Foundation (2016M590686), and the National Science Foundation for Distinguished Young Scholars of China (61425021).

Notes and references

1 M. Enserink, *Science*, 2001, **294**, 490–491.
2 R. Schuch, D. Nelson and V. A. Fischetti, *Nature*, 2002, **418**, 884–889.
3 C. Terry, A. Shepherd, D. S. Radford, A. Moir and P. A. Bullough, *PLoS One*, 2011, **6**, e23801.
4 M. J. Hajipour, K. M. Fromm, A. A. Ashkarran, D. Jimenez de Aberasturi, I. R. de Larramendi, T. Rojo, V. Serpooshan, W. J. Parak and M. Mahmoudi, *Trends Biotechnol.*, 2012, **30**, 499–511.
5 R. Das, A. K. Goel, M. K. Sharma and S. Upadhyay, *Biosens. Bioelectron.*, 2015, **74**, 939–946.
6 J. Kell, L. Page, S. Tan, I. Charlebois, M. Boissinot, M. LeClercand and B. Simard, *Nanoscale*, 2011, **3**, 3747–3754.
7 R. Mabry, K. Brasky, R. Geiger, C. R. Jr, G. B. Hubbard, S. Leppla, J. L. Patterson, G. Georgiou and B. L. Iverson, *Clin. Vaccine Immunol.*, 2006, **13**, 671–677.
8 P. R. Sajanlal and T. Pradeep, *Nanoscale*, 2012, **4**, 3427–3437.
9 I. Lee, W. K. Oh and J. Jang, *J. Hazard. Mater.*, 2013, **252–253**, 186–191.

10 Q. Li, K. Sun, K. Chang, J. Yu, D. T. Chiu, C. Wu and W. Qin, *Anal. Chem.*, 2013, **85**, 9087–9091.
11 H. Zhang, H. Song, H. Yu, S. Li, X. Bai, G. Pan, Q. Dai, T. Wang, W. Li and S. Lu, *Appl. Phys. Lett.*, 2007, **90**, 103103.
12 S. I. Klink, L. Grave, D. N. Reinhoudt, F. C. J. M. V. Veggel, M. H. V. Werts, F. A. J. Geurts and J. W. Hofstraat, *J. Phys. Chem. A*, 2000, **104**, 5457–5468.
13 Z. Li, P. Li and Q. Xu, *et al.*, *Chem. Commun.*, 2015, **51**(53), 10644–10647.
14 K. Ai, B. Zhang and L. Lu, *Angew. Chem., Int. Ed.*, 2009, **48**, 304–308.
15 C. Tan, Q. Wang and C. C. Zhang, *Anal. Chem.*, 2011, **47**, 12521–12523.
16 B. Ma, F. Zeng, F. Zheng and S. Wu, *Analyst*, 2011, **136**, 3649–3655.
17 Y. Zhang, B. Li, H. Ma, L. Zhang, H. Jiang, H. Song, L. Zhang and Y. Luo, *J. Mater. Chem. C*, 2016, **4**, 7294–7301.
18 W. K. Oh, Y. S. Jeong, J. Song and J. Jang, *Biosens. Bioelectron.*, 2011, **29**, 172–177.
19 J. Ryu, E. Lee, K. Lee and J. Jang, *J. Mater. Chem. B*, 2015, **3**, 4865–4870.
20 X. Lu, P. Wang, Y. Wang, C. Liu and Z. Li, *Adv. Mater. Technol.*, 2016, **1**, 1600024.
21 X. Jiang, F. L. Wong, M. K. Fung and S. T. Lee, *Appl. Phys. Lett.*, 2003, **83**, 1875.
22 S. Chu, M. Olmedo, Z. Yang, J. Kong and J. Liu, *Appl. Phys. Lett.*, 2008, **93**, 181106.
23 D. Ick Son, H. Yeon Yang, T. Whan Kim and W. Il Park, *Appl. Phys. Lett.*, 2013, **102**, 021105.
24 Q. Wan, Q. H. Li, Y. J. Chen, T. H. Wang, X. L. He, J. P. Li and C. L. Lin, *Appl. Phys. Lett.*, 2004, **84**, 3654.
25 G. Brammertz, M. Buffière, S. Oueslati, H. ElAnzeery, K. Ben Messaoud, S. Sahayaraj, C. Köble, M. Meuris and J. Poortmans, *Appl. Phys. Lett.*, 2013, **103**, 163904.
26 X. Wang, J. Zhou, J. Song, J. Liu, N. Xu and Z. L. Wang, *Nano Lett.*, 2007, **6**, 2768–2772.
27 Z. L. Wang and J. Song, *Science*, 2006, **312**, 242–246.
28 J. Luo, S. Zhao, P. Wu, K. Zhang, C. Peng and S. Zheng, *J. Mater. Chem. C*, 2015, **3**, 715–723.
29 O. Arslan, L. Belkoura and S. Mathur, *J. Mater. Chem. C*, 2015, **3**, 11965–11973.
30 A. Aboulaich, C. M. Tilmaciu, C. Merlin, C. Mercier, H. Guilloteau, G. Medjahdi and R. Schneider, *Nanotechnology*, 2012, **23**, 105–108.
31 J. Zhang, R. Zhang, L.-H. Zhao and S.-Q. Sun, *CrystEngComm*, 2012, **14**, 613–619.
32 H. M. Xiong, *Adv. Mater.*, 2013, **25**, 5329–5335.
33 X. Tang, E. S. G. Choo, L. Li, J. Ding and J. Xue, *Chem. Mater.*, 2010, **22**, 3383–3388.
34 S. K. Arya, S. Saha, J. E. Ramirez-Vick, V. Gupta, S. Bhansali and S. P. Singh, *Anal. Chim. Acta*, 2012, **737**, 1–21.
35 D. Zhao, H. Song, L. Hao, X. Liu, L. Zhang and Y. Lv, *Talanta*, 2013, **107**, 133–139.
36 K. Singh, G. R. Chaudhary, S. Singh and S. K. Mehta, *J. Lumin.*, 2014, **154**, 148–154.
37 D. A. Long, *J. Raman Spectrosc.*, 2004, **35**, 905.
38 Z. Mekhalif, L. Massi, F. Guittard, S. Geribaldi and J. Delhalle, *Thin Solid Films*, 2002, **405**, 186–193.
39 E. J. Cho and S. J. Oh, *Phys. Rev. B: Condens. Matter Mater. Phys.*, 1999, **59**, R15613.
40 S. Kumar, R. Prakash, R. J. Choudhary and D. M. Phase, *Mater. Res. Bull.*, 2015, **70**, 392–396.
41 Y. Lu and B. Yan, *J. Mater. Chem. C*, 2014, **2**, 7411–7416.
42 N. Wartenberg, O. Raccurt, D. Imbert, M. Mazzanti and E. Bourgeatlami, *J. Mater. Chem.*, 2013, **1**, 2061–2068.
43 M. D. Yilmaz, S. H. Hsu, D. N. Reinhoudt, A. H. Velders and J. Huskens, *Angew. Chem.*, 2010, **49**, 5938–5941.
44 Y. Zhang, B. Li, H. Ma, L. Zhang and Y. Zheng, *Biosens. Bioelectron.*, 2016, **85**, 287–293.
45 H. Tan, Q. Li, C. Ma, Y. Song, F. Xu, S. Chen and L. Wang, *J. Nanopart. Res.*, 2013, **16**, 1–11.
46 K. M. L. Taylor and W. Lin, *J. Mater. Chem.*, 2009, **19**, 6418–6422.
47 W. J. Rieter, K. M. Taylor and W. Lin, *J. Am. Chem. Soc.*, 2007, **129**, 9852–9853.
48 A. G. Casado, L. C. Rodriguez, E. A. Hernandez and J. L. Vilchez, *J. Chromatogr. A*, 1996, **726**, 133–139.
49 G. L. Long and J. D. Winefordner, *Anal. Chem.*, 1983, 712A–724A.
50 L. A. Carreira, M. Rizk, Y. El-Shabrawy, N. A. Zakhari and S. S. Toubar, *J. Pharm. Biomed. Anal.*, 1995, **13**, 1331–1337.
51 A. Habenschuss and F. H. T. Spedding, *J. Chem. Phys.*, 1980, **70**, 442–450.